ACS Catalysis

Research Article

pubs.acs.org/acscatalysis

Oxidative Dehydrogenation of Ethane with CO_2 over Flame-Made Ga-Loaded TiO_2

Rajesh Koirala,[†] Robert Buechel,[†] Frank Krumeich,[‡] Sotiris E. Pratsinis,[†] and Alfons Baiker*[,‡]

[†]Particle Technology Laboratory, Department of Mechanical and Process Engineering, ETH Zurich, Sonneggstrasse 3, CH-8092 Zurich, Switzerland

[‡]Department of Chemistry and Applied Biosciences, ETH Zurich, Hönggerberg, HCI, Vladimir-Prelog Weg 1, CH-8093 Zurich, Switzerland

ABSTRACT: The influence of the Ga content (0−17 wt %) on the structural properties and the catalytic behavior of flame-synthesized TiO_2-supported gallium oxide in the oxidative dehydrogenation of ethane (ODHE) has been investigated in a continuous tubular microreactor using CO_2 as a mild oxidant. The gallium oxide−titania powders consisted of nonporous spherical particles of about 10 nm average diameter, as indicated by HRTEM and X-ray line broadening, and had a specific surface area of about 120 m^2/g. XRD showed no reflections corresponding to Ga_2O_3 in the as-prepared samples, indicating high dispersion of the Ga constituent. At higher Ga loading (>14 wt %) stronger acidic sites became prominent, as indicated by NH_3-TPD and DRIFTS. The ethene yield increased with Ga loading up to about 10 wt %. The molar CO_2/C_2H_6 ratio in the feed, reaction temperature, and space velocity were decisive parameters for achieving maximum ethene yield. The ethene yield achieved was 22% using a CO_2/C_2H_6 ratio of 2.5, 700 °C, and a space velocity of 6000 L/((kg of cat.) h), corresponding to 57% ethane conversion at 38% selectivity to ethene. After reaction (1 h on stream) all catalysts showed significant coking and a loss of surface area depending on the Ga content. Catalysts with higher Ga content were more resistant toward sintering but showed more severe coking due to the presence of stronger acidic sites. Raman spectroscopy revealed that all spent catalysts were covered with both D- and G-type carbon. Both carbon deposition and reduction of catalyst surface area led to a significant decrease in activity with time on stream, while the selectivity to ethene increased up to above 70%. The catalysts could efficiently be regenerated by exposing them for 10 min to air at a reaction temperature of 700 °C, providing a base for the development of a dynamic process consisting of alternative ODHE/regeneration cycles.

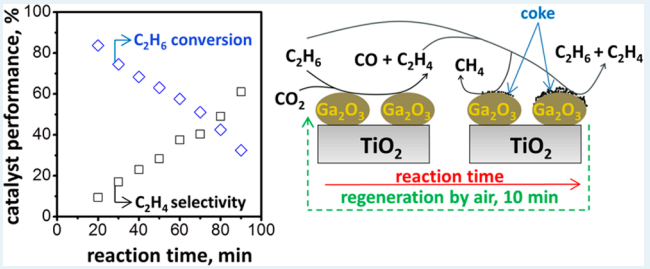

KEYWORDS: *oxidative dehydrogenation, ethane, carbon dioxide, gallium oxide, flame spray pyrolysis*

1. INTRODUCTION

One of the most important feedstocks in chemical industry is ethene, a building block for the synthesis of commercially important products, such as polyethylene, ethylene oxide, styrene, acetaldehyde, vinyl acetate, ethylene di(chloride/bromide), ethanol, ethylbenzene, and many more.[1−3] The demand for these materials is growing due to the rising global market.[3] Currently, ethene is produced mostly by steam cracking of naphtha and ethane. These raw materials constitute approximately 70% of the production cost, resulting in million tons of CO_2 emission worldwide.[4] The cracking process requires relatively high temperatures (>1000 °C) and severely suffers from coking, which forces a complete shutdown of the operation for periodic cleaning.[4] As a consequence, there is a compelling need for the development of an alternative, cost-effective process. Thermal dehydrogenation of ethane can also effectively produce ethene at high temperatures (50% conversion, 720 °C); however, it suffers from uncontrollable side reactions as well as rapid coking.[5]

$$C_2H_6 \leftrightarrow C_2H_4 + H_2 \quad \Delta H^\circ_{298} = +136.5\ \text{kJ/mol} \qquad (1)$$

Therefore, the use of catalysts to minimize the aforementioned problems while achieving high conversion and selectivity is of great technological and economical interest. As an alternative, oxidative dehydrogenation of ethane (ODHE) has been proposed over thermal dehydrogenation. The current state of ODHE has been covered in a recent review, where common principles and mechanistic aspects are discussed.[2]

$$C_2H_6 + 0.5O_2 \leftrightarrow C_2H_4 + H_2O$$
$$\Delta H^\circ_{298} = -105.3\ \text{kJ/mol} \qquad (2)$$

This reaction is highly favored even at lower temperatures (400−600 °C). However, the process is exothermic, requiring efficient removal of the excess heat. Moreover, though oxygen effectively oxidizes the deposited carbon from the catalyst surface, it also decreases ethene selectivity by deep oxidation. Therefore, the use of a milder oxidant is preferred to overcome

Received: May 20, 2014
Revised: November 17, 2014
Published: December 15, 2014

DOI: 10.1021/cs500685d
ACS Catal. 2015, 5, 690−702

the low selectivity. Recently, CO_2 has been applied as a soft oxidant for oxidative dehydrogenation of various alkanes (ethane, propane) and ethylbenzene and methane coupling for ethene production.[6] Such a strategy to utilize CO_2 for commercial purposes is attractive and promising, as it can be used for the synthesis of valuable products rather than releasing it into the atmosphere.

Nakagawa et al.[7] studied a series of metal oxides and found that Ga_2O_3 is an efficient catalyst for ODHE with a yield (18.6%) doubled in the presence of CO_2 than in its absence (9%). Moreover, the ethene yield increased from about 3 to 25% with increasing Ga_2O_3 surface area (from about 1 to 50 m^2/g).[8] The catalytic performance of Ga_2O_3 supported on TiO_2 was shown also to be superior to that on ZrO_2, ZnO, Al_2O_3, and SiO_2 supports for ODHE with CO_2. However, the ethene yield decreased remarkably when the Ga_2O_3/TiO_2 catalyst was subjected to a time on stream test, reaching a value of ~2% within 3 h due to carbon deposition. Surface properties, such as acidity and basicity of Ga_2O_3 (amphoteric), are believed to play a key role in the catalyst performance.[8−10] In addition, the slightly acidic CO_2, upon coming in contact with the Ga_2O_3 surface, may alter its acidic/basic properties. To reduce coke deposition, tuning the acidity of Ga_2O_3 by addition of basic metal oxides (e.g., potassium oxide) decreased the alkane conversion.[11] Shen et al.[12] reported that higher Si/Al ratio HZSM-5-supported Ga_2O_3 catalysts are more resistant toward deactivation. They achieved an ethane conversion of 15% at 94% ethene selectivity after 70 h of reaction. The enhancement of the selectivity was attributed to a reduction of the catalyst's acidity suppressing undesired side reactions. The amounts of deposited coke on Ga_2O_3/HZSM-5(97) and β-Ga_2O_3 catalysts were virtually the same. However, the latter catalyst, which had a 10 times lower surface area, deactivated more quickly, resulting in blocked active sites. Gallium oxide based catalysts have already shown potential in various dehydrogenation reactions of alkanes; however, the reactions are crippled by coking.[13,14] Thus, further research is essential to make such catalysts suitable for an efficient and stable alkane dehydrogenation process.

Flame spray pyrolysis (FSP)[15] has proven to be a versatile material synthesis technique, with great control over particle morphology[16] and various other physical properties favorable for catalytic applications.[17] Moreover, it is a single-step process, with fast and high production rates unlike those of most conventional catalyst preparation routes. Flame-made particles experience rapid cooling due to the short flame reaction zone,[18] which prevents further sintering. In this process novel composition of mixed oxide phases can form[19] along with well-defined structures.[20] The potential of this method for the synthesis of catalytic materials has been proven in tailoring textural properties as well as dispersion and spatial distribution of active components.[21]

With this in mind we synthesized a series of flame-made Ga_2O_3/TiO_2 catalysts with different Ga loadings and investigated their structural properties and catalytic potential for ODHE using CO_2 as a mild oxidant. The main focus was the influence of the Ga loading and reaction conditions (CO_2/C_2H_6 feed ratio, temperature, space velocity) on the performance, deactivation, and regeneration behavior of these catalysts.

2. EXPERIMENTAL SECTION

2.1. Catalyst Preparation. Rapid and scalable single-nozzle FSP[15] was used for catalyst synthesis.[22] The primary flame was created using premixed CH_4 and O_2 (>99.9%, Pangas) with flow rates of 1 and 2 L/min, respectively. Gallium acetylacetonate (99.99%, Sigma-Aldrich) and titanium isopropoxide (TTIP) (97%, Sigma-Aldrich) were dissolved in xylene to form precursor solutions with a total metal concentration of 0.45 M, which were injected at 5 mL/min by a syringe pump (Lambda, VIT-FIT) through the FSP nozzle and dispersed into fine droplets by coflowing 5 L/min of O_2 (>99.9%, Pangas) and maintaining a pressure drop of 2 bar at the nozzle tip.[15] Gas flow rates were regulated by mass flow controllers (Bronkhorst). The resulting powders were collected on water-cooled glass fiber filters (Whatman GF 6, 25.7 cm in diameter) 54 cm above the burner with the aid of a vacuum pump (Busch, Seco SV 1040C). In addition to Ga/TiO_2 catalysts, pure Ga_2O_3 and TiO_2 were also synthesized as reference materials using FSP. Commercial Ga_2O_3 (Alfa Aesar, 99.99% metal basis) was used as received as a reference.

2.2. Characterization. Nitrogen adsorption−desorption isotherms were measured using a Micromeritics Tristar 3000 instrument at 77 K. Samples were pretreated at 150 °C for 1 h under a continuous flow of nitrogen to remove volatile impurities. The Brunauer−Emmett−Teller (BET) method was utilized to determine the specific surface area (SSA) of the nanoparticles. Average particle diameters were estimated from the SSAs by $d_p = 6/(\rho_{av}*SSA)$. The average density ρ was calculated using weighted densities of Ga_2O_3 (5.88 g/cm^3), anatase (3.84 g/cm^3), and rutile TiO_2 (4.26 g/cm^3), respectively.

X-ray diffraction (XRD) was performed on a Bruker D8 Advance diffractometer (40 kV, 40 mA, Cu Kα) over the 2θ range of 10−70°. Average crystal sizes were estimated using the TOPAS Rietveld method, with measurement of the peak widths, and the fraction of rutile in TiO_2 was calculated using the formula given by Spur and Myer:[23]

$$\text{wt \% rutile} = \left(1 + \frac{0.8I_A}{I_R}\right)^{-1} \quad (3)$$

where I_A and I_R are the intensities of anatase and rutile obtained from XRD measurements at 2θ = 25 and 27°, respectively.

Acidic sites on the catalyst surfaces were probed by NH_3 temperature programmed desorption (TPD) using a Micromeritics Autochem II 2920 instrument. The samples (ca. 100 mg) were placed in a U-shaped glass tube, heated to 400 °C (10 °C/min) in a 5% O_2/He flow (20 mL/min) (Pangas) and held at this temperature for 30 min. Then the gas flow was switched to He (Pangas, 99.999%) before the temperature was lowered to 50 °C. After this pretreatment, 10 mol % NH_3/Ar (Pangas) was passed over the samples with a flow rate of 20 mL/min for 90 min and then switched back to He flow and ramped to 100 °C (10 °C/min) and held at this temperature for 20 min. Finally, NH_3-TPD was performed by heating the sample to 840 °C with a heating rate of 10 °C/min and at a He flow rate of 20 mL/min. The evolved gases were monitored by a mass spectrometer (Pfeiffer Vacuum, Thermostar, m/z = 15). CO_2-TPD measurements were performed following the aforementioned process, but using CO_2 (m/z = 44) instead of NH_3 to probe the basic sites of the samples.

Diffuse reflectance infrared Fourier transform spectroscopy (DRIFTS) of all fresh powders and commercial Ga_2O_3 was performed on a Vertex 70v spectrometer (Bruker Optics). Spectra were obtained by averaging 100 scans at 4 cm^{-1} resolution. The powder samples were placed in an in situ

DOI: 10.1021/cs500685d
ACS Catal. 2015, 5, 690−702

DRIFTS cell which was heated to 400 °C in 5% O_2/He (Pangas) and held at this temperature for 30 min before the temperature was lowered to 40 °C under He flow. For NH_3 adsorption the gas was switched to 10 mol % NH_3 in Ar, which was passed over the sample for 15 min. Afterward the sample was flushed with He for 15 min before measuring the spectra.

Raman spectroscopy (Renishaw InVia Raman microscope) analysis of both the fresh and spent powders was performed with a 514 nm laser at ranges of 100−800 and 100−1800 cm^{-1}, respectively. The laser power was set to 10% with an exposure time of 10 s.

Thermal analyses of spent catalysts were carried out using a thermogravimetric analyzer (TGA/SDTA851e, LF/1100 °C, Mettler Toledo AG) and a mixture of 40 mL/min O_2 and 10 mL/min Ar as reactant gas, which was passed over the samples to oxidize the deposited carbon. The evolving gases were monitored by an attached well-calibrated mass spectrometer (Quadstar 422, Balzers) to identify the released volatiles from the sample. The same amounts of sample (~28 mg) were taken for all of the analyses.

High-resolution transmission electron microscopy (HRTEM) was performed on a Tecnai F30 microscope (FEI; FEG cathode, at 300 kV, point resolution approximately 2 Å). Scanning transmission electron microscopy (STEM) and energy-dispersive X-ray spectroscopy (EDXS) studies were done using an aberration-corrected, dedicated STEM (Hitachi HD-2700CS) apparatus equipped with a probe corrector (CEOS). STEM imaging was performed at an acceleration potential of 200 kV (electron gun: cold-field emitter) detecting incoherently scattered electrons with a high-angle annular dark-field detector (HAADF-STEM). An EDX spectrometer (Gemini system, EDAX) mounted in the electron column above the sample facilitated recording spectra of selected spots and elemental distribution maps (recording times ca. 30 min).

2.3. Catalytic Studies. Reactions were carried out at atmospheric pressure in a tubular quartz fixed-bed microreactor of 4 mm inner diameter, which was contracted to 2 mm after the catalyst bed. The catalyst bed consisted of a mixture of 150 mg of catalyst (80−140 μm mesh) and 50 mg of inert SiC (160−190 μm mesh), which was fixed at the center of the reactor with quartz wool. The catalyst bed length was ca. 2 cm. If not otherwise stated, the reactant gases, ethane (99.5% PanGas) and carbon dioxide (99.95% PanGas), were passed at a total flow rate of 15 mL/min through the catalyst bed. Flow rates were regulated by calibrated mass flow controllers (Brooks). If not otherwise stated, the molar feed gas ratio CO_2/C_2H_6 was 2.5.

The reactor was placed in a temperature-controlled electrically heated furnace and heated to the reaction temperature (700 °C at 10 °C/min in standard experiments), which was monitored with two thermocouples placed inside the reactor touching both the inlet and outlet of the catalyst bed. Generally, in catalytic runs the temperature difference between the inlet and outlet was <4 °C. Reactor effluent gas lines were heated to 120 °C with heating tapes to prevent possible condensation. Online gas chromatography (HP-PLOT Q column 30 m long, 0.32 mm in diameter and 0.2 μm film thickness fitted with TCD and FID, Agilent Technologies) was utilized to analyze gases in the product stream. A quadrupole mass spectrometer (MS; Pfeiffer Vacuum, Thermostar GSD 300) and a non-dispersive infrared analyzer for measuring CO and CO_2 (ABB Uras 26) were also used to complement the GC analysis. Cold water traps were used to condense water formed during the reaction. All of the catalytic data are reported after 1 h reaction (time on stream) unless otherwise noted. C_2H_6 conversion, C_2H_4 selectivity and C_2H_4 yield were calculated as

$$C_2H_6\ \text{conversion}\ (\%) = \frac{\text{moles of}\ C_2H_6\ \text{consumed}}{\text{moles of}\ C_2H_6\ \text{in the feed}} \times 100 \quad (4)$$

$$C_2H_4\ \text{selectivity}\ (\%) = \frac{\text{moles of}\ C_2H_4\ \text{produced}}{\text{moles of}\ C_2H_6\ \text{consumed}} \times 100 \quad (5)$$

$$C_2H_4\ \text{yield}\ (\%) = \frac{C_2H_6\ \text{conversion}\ (\%) \times C_2H_4\ \text{selectivity}\ (\%)}{100} \quad (6)$$

H_2 concentration was not measured during the reaction. Catalyst regenerability experiments were performed using two different oxidants, CO_2 and synthetic air ($O_2 \leq 20\%$ balance N_2), keeping the aforementioned reaction conditions constant. Synthetic air was utilized, after 90 min reaction for 10 min, to remove coke from the catalyst's surface.

3. RESULTS AND DISCUSSION

3.1. Textural and Structural Properties. Figure 1a shows the XRD patterns of as-prepared flame-made Ga_2O_3, TiO_2, and various gallium-loaded TiO_2 catalysts. Pure flame-made Ga_2O_3 showed low-intensity reflections at about 2θ = 32, 35, and 46°

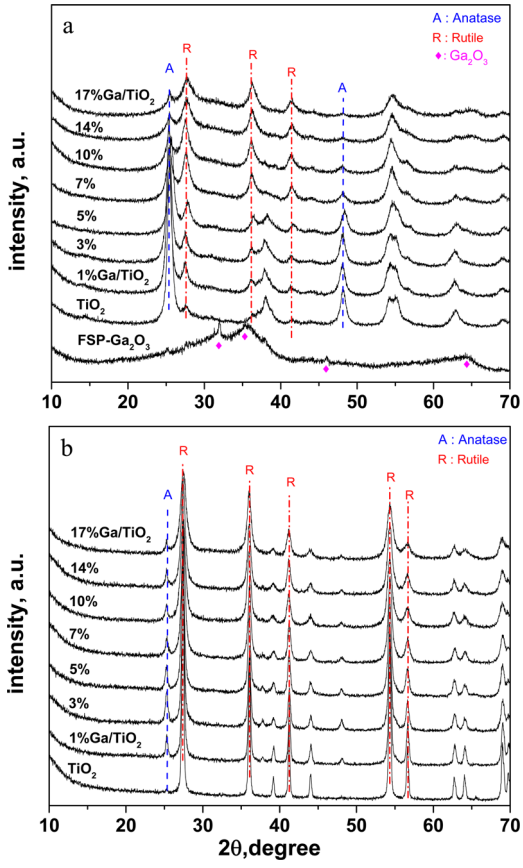

Figure 1. XRD patterns of flame-made (a) as-prepared pure Ga_2O_3, TiO_2, and various gallium-loaded TiO_2, and (b) spent gallium-loaded TiO_2 after 1 h on stream. Conditions: CO_2/C_2H_6 ratio, 2.5; space velocity, 6000 L/((kg of cat.) h); temperature, 700 °C.

DOI: 10.1021/cs500685d
ACS Catal. 2015, 5, 690−702

in addition to some broader humps prominent at $2\theta = 64°$, indicating that a significant fraction of this material was amorphous. TiO_2 mainly consisted of anatase (>80%). However, upon introduction of gallium, the intensity of the anatase reflections decreased while the rutile reflections increased, indicating that Ga promoted rutile formation. In similar catalysts prepared by laser-induced pyrolysis, the anatase to rutile transformation was observed only upon calcination above 900 °C.[24] This promotion of the anatase−rutile transformation has been attributed to the similar ionic radii of Ga^{3+} and Ti^{4+}, i.e. 0.62 and 0.61 Å, respectively, favoring substitution[25] of Ti^{4+} by Ga^{3+} in the TiO_2 lattice similar to the case for Al^{3+} in titania.[26] Vemury et al.[27] and Teoh et al.[28] also had reported the replacement of titanium with slightly larger metal ions, i.e. Sn^{4+} = 0.69 and Fe^{3+} = 0.64 Å, respectively, during flame synthesis of doped TiO_2. No reflections indicative of Ga_2O_3 or mixed oxides were observed in any of the Ga-loaded TiO_2 catalysts, indicating that the Ga component was highly dispersed. However, on comparison of the pattern of flame-made pure Ga_2O_3 to that of the Ga/TiO_2 powders, in the latter a small, broad hump was discernible at about $2\theta = 64°$ whose intensity increased with increasing gallium loadings. This could be attributed to amorphous Ga_2O_3 at these loadings.

After ODHE, the rutile content of the TiO_2 was >90 wt % (Figure 1b). The highest rutile content was observed for pure TiO_2 (~100%), while for the Ga-loaded samples it was in the range of 90−98 wt %. The addition of Ga increased the catalyst's resistance to sintering. This is indicated by the decreasing rutile crystal size from 65 to 20 nm with increasing gallium content from 0 to 17 wt %. The rutilization occurring during ODHE can be attributed to the favorable reducing conditions at high temperature (700 °C).[29] Complete rutilization was reported for wet-made powders containing gallium and titanium after calcination at >950 °C.[30] The absence of rutilization in as-prepared wet-made catalysts is attributed to the different interactions of the gallium and titanium species in the liquid and gas phases and also to the exposure to different temperatures during their preparation.[30,31]

Figure 2a shows nitrogen adsorption−desorption isotherms of representative samples. The isotherms of all powders showed the same characteristic shape, indicating that particles were nonporous.[22] The hysteresis at high P/P_0 is due to the interstitial void volumes of the powders. TEM images of all samples indicated nearly spherical particles, as exemplified by the representative examples of pure TiO_2 and 10 wt % Ga-loaded TiO_2 (Figure 2b,c).

Figure 3 shows the HAADF-STEM image and the elemental maps of gallium and titanium of as-prepared 10% Ga/TiO_2 catalysts. The serially measured elemental maps reveal the presence of well-distributed gallium (red) over titanium (green). Moreover, the EDX spectrum (not shown) on every measured spot contained the peaks of gallium and titanium simultaneously, providing another indication that probably part of the Ga^{3+} ions substitute some Ti^{4+} ions in the TiO_2 lattice, similar to the case for Al^{3+}.[26]

In order to gain information about the surface acidic and basic sites, we applied NH_3- and CO_2-TPD measurements. In their pure form both oxide constituents, TiO_2 and Ga_2O_3, are amphoteric, possessing acidic and basic sites.[32] The NH_3-TPD profiles (Figure 4a) show that the pure TiO_2 and the Ga-loaded TiO_2 possess acidic sites of various strengths. The strongest acidic sites (high-temperature peak marked with dotted lines in the NH_3-TPD) are most prominent on the higher Ga-loaded

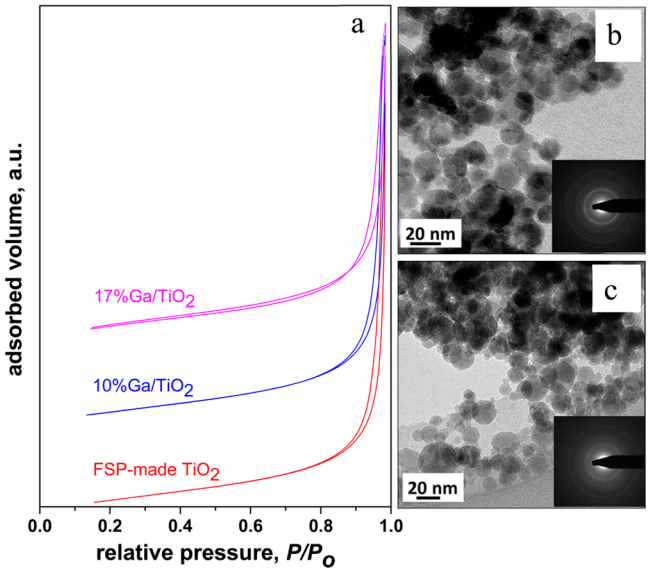

Figure 2. (a) Nitrogen adsorption−desorption isotherms of FSP-made TiO_2, 10% Ga/TiO_2, and 17% Ga/TiO_2 and (b, c) TEM images of as-prepared (b) TiO_2 and (c) 10% Ga/TiO_2.

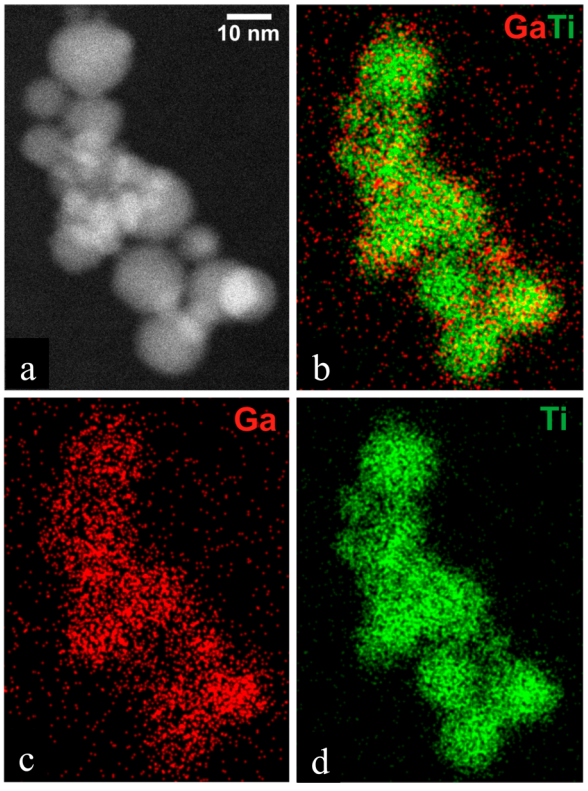

Figure 3. (a) HAADF-STEM image and (b) combined map of the 10% Ga/TiO_2 sample. The elemental maps of Ga (c) and Ti (d) reveal a homogeneous distribution of both elements. At every measured spot, the EDX spectrum (not shown here) shows the peaks corresponding to Ga and Ti simultaneously.

catalysts (14%, 17%, and the pure Ga_2O_3). Deconvolution of the TPD profiles of 10% and 17% Ga-loaded TiO_2 catalysts showed multiple peaks with obvious increase of high-temperature peaks, indicating promotion of medium to strong acidic sites with increasing Ga loading (Figure 4b). These strong acidic sites are assumed to be mainly responsible for the

DOI: 10.1021/cs500685d
ACS Catal. 2015, 5, 690−702

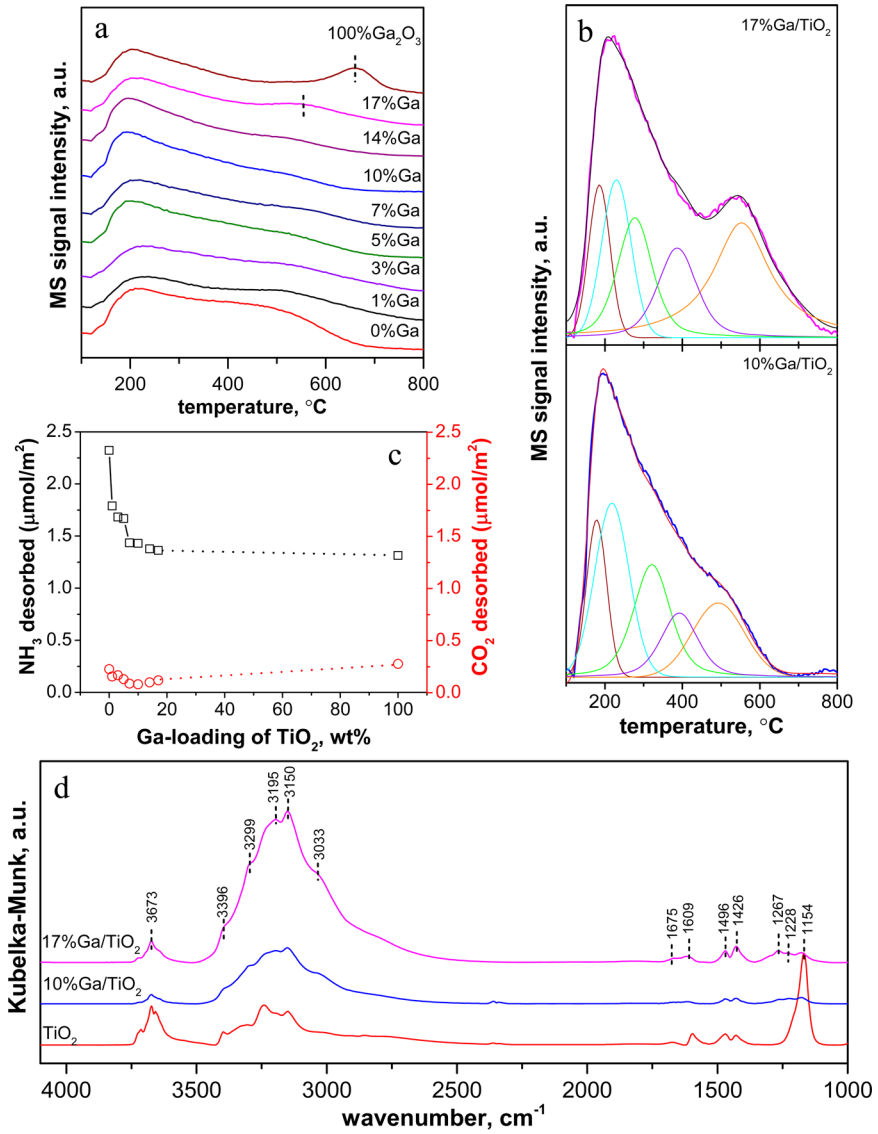

Figure 4. Characterization of acidic and basic sites of Ga-loaded TiO_2: (a) NH_3-TPD profiles and (b) NH_3-TPD profiles of 10% and 17% Ga/TiO_2 catalysts deconvoluted with Gaussian function. (c) Desorbed amount of NH_3 and CO_2 during TPD analysis. (d) DRIFT spectra of FSP-made pure TiO_2 and 10% and 17% Ga-loaded TiO_2 after NH_3 adsorption.

enhanced coke deposition at higher gallium loadings.[33,34] The NH_3 uptake of the pure flame-made TiO_2 was 2.3 μmol/m^2, which is within the range of previously reported values 3.2[35] and 1.5 μmol/m^2 [36] and close to that reported by Gervasini and Auroux (2.5 μmol/m^2),[37] on differently synthesized and pretreated TiO_2. Although at higher Ga loadings new strong acid sites appeared, a decrease in the population of acidic sites was observed upon addition of gallium, in agreement with the observation of Petre et al.[10] in their pyridine adsorption experiments. This decrease is prominent for gallium loadings up to about 8%; a further increase of Ga loading did not have a significant effect on the total population of acidic sites, probably due to the appearance of strong acid sites, as evidenced in the NH_3-TPD profiles. Figure 4c indicates that the population of basic sites changed relatively little with the gallium loading. The CO_2 uptakes by TiO_2 (0.23 μmol/m^2) and Ga_2O_3 (0.28 μmol/m^2) are close to those reported by Gervasini and Auroux.[37] In Figure 4d, DRIFT spectra of flame-made pure TiO_2 and various Ga-loaded TiO_2 catalysts are presented. Formation of new bands and also band widening with increasing gallium content indicates alteration of the distribution of the different acidic sites (Brønsted and Lewis sites) when TiO_2 is loaded with gallium. The multiple bands at 3396, 3299, 3195, and 3150 cm^{-1} can be associated with stretching vibrations (both asymmetric and symmetric ν_{NH}) of NH_3 on the TiO_2 surface.[38] Moreover, the spectra around 3673[39] and 3033[40] cm^{-1} indicate the existence of residual OH groups on the pretreated Ga/TiO_2 surface. The bands at 1496 and 1426 cm^{-1} are assigned to Brønsted acid sites,[41] whereas bands at 1675, 1609, 1228, and 1154 cm^{-1} arise from coordinatively adsorbed NH_3 on Lewis acid sites.[38] Upon Ga loading of the TiO_2, a new distinct band appeared around 1267 cm^{-1}, which is attributed to NH_3 bonding on Lewis acid sites of the Ga_2O_3 or mixed oxides (Ga/TiO_2).[42] This band became more prominent with increasing Ga content. From the DRIFT spectra and NH_3-TPD measurements we infer that with increasing Ga loading the concentration of coordinatively unsaturated Ga^{3+} on the catalyst surface increases,[43,44] as indicated by the formation of new bands and the creation of strong acid sites.

DOI: 10.1021/cs500685d
ACS Catal. 2015, 5, 690−702

Figure 5a shows the SSA of all as-prepared and corresponding spent catalysts. All as-prepared Ga-loaded

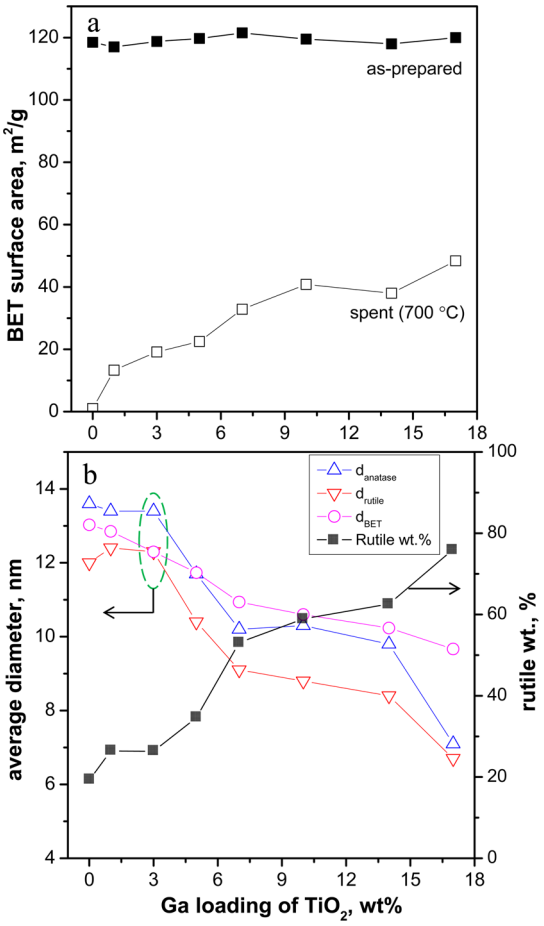

Figure 5. (a) Comparison of specific surface areas of as-prepared and spent (after 1 h on stream at 700 °C) Ga/TiO_2 catalysts. (b) Average particle diameter and rutile content (wt %) of TiO_2 in various as-prepared Ga/TiO_2 catalysts.

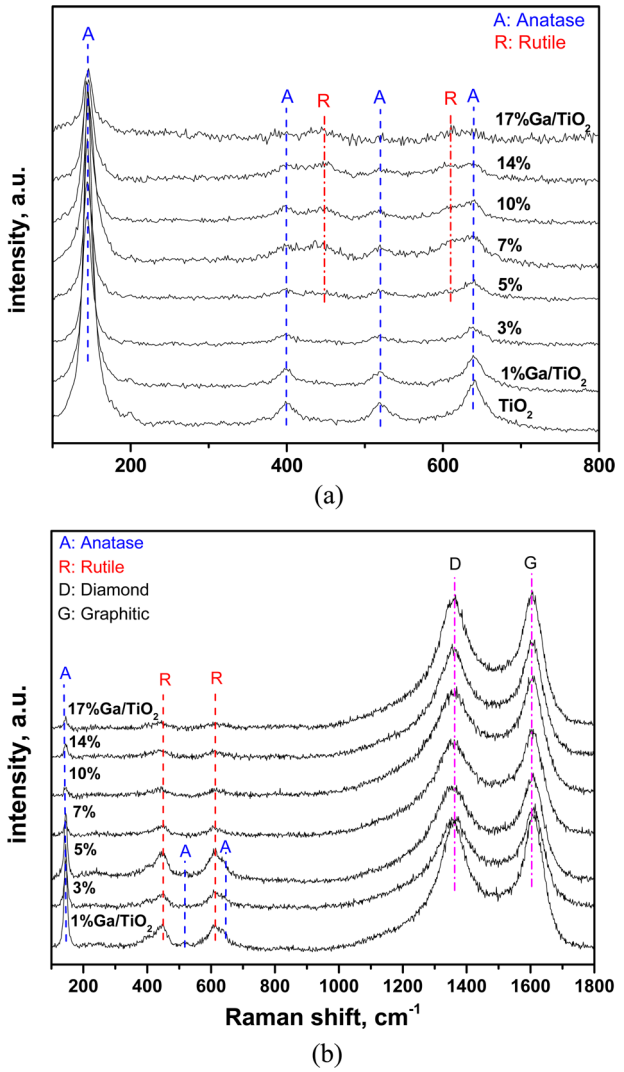

Figure 6. Raman spectra of (a) as-prepared and (b) spent (after 1 h on stream) Ga/TiO_2 catalysts.

TiO_2 had an SSA around 120 m^2/g. The rapid particle production in the flame (low residence time, high temperature, fast quenching) results in higher surface area because further particle growth is prevented.[45] However, a dramatic loss of surface area was observed for spent catalysts (after 1 h on stream at 700 °C). The presence of Ga, however, mitigated that loss of SSA. As an example, the SSAs of spent TiO_2 and 17% Ga/TiO_2 were 1 and 40 m^2/g, respectively.

In Figure 5b the average particle diameters estimated from BET and X-ray diffraction of as-prepared catalysts are plotted as a function of the Ga content. The average particle sizes estimated using these methods show a similar trend: they decline with increasing gallium content of the mixed oxide. The average crystal size of both anatase and rutile phases continuously decreased with increasing Ga loading, however, they attained similar values (~7 nm) at a loading of 17 wt %. The rutile content in as-prepared catalysts was about 20 wt %, which increased with Ga loading to reach, for example, about 76% at 17 wt % Ga.

Raman spectroscopy of as-prepared TiO_2 showed typical bands belonging to anatase at about 144, 400, 515, and 636 cm^{-1}, whereas no bands due to rutile were identified (Figure 6a).[46] However, with increasing Ga loading, some weak broad signals evolved at about 446 and 609 cm^{-1}, indicating the presence of rutile. No bands of Ga_2O_3 were observed in the Ga-loaded TiO_2 powders, in agreement with XRD (Figure 1a). In Figure 6b Raman spectra of all spent catalysts (after 1 h on stream) are shown. Both anatase and rutile bands were observed along with bands belonging to diamond (D) and graphitic (G) carbon at 1356 and 1605 cm^{-1}, respectively.[47]

Significant changes in the intensities of Raman bands due to TiO_2 were observed in spent catalysts (after 1 h on stream) depending on the gallium content (Figure 6b). Raman band intensities of anatase at 144, 514, and 642 cm^{-1} decreased, while those of rutile increased with increasing gallium content up to 5 wt %. At higher loadings, the intensity of the corresponding bands decreases in comparison to carbon peaks but their ratio (rutile/anatase) remains the same.

At 7 wt % Ga, bands at 514 and 642 cm^{-1} completely disappeared, while bands of rutile at 445 and 615 cm^{-1} were still present, though at low intensities. No Raman bands indicative of Ga_2O_3 or mixed oxides were observed in spent catalysts, in agreement with XRD (Figure 1b), confirming the high dispersion of Ga even at high loadings. Figure 6b also depicts the Raman bands of D and G carbon. While on pure TiO_2 predominantly graphitic carbon (not shown) was

DOI: 10.1021/cs500685d
ACS Catal. 2015, 5, 690−702

deposited after 1 h on stream, on Ga-loaded TiO_2 the distribution between D and G carbon was more equalized with an estimated ratio of around 1.6.

3.2. Catalytic Performance. Figure 7a shows the catalytic performance of the various Ga/TiO_2 catalysts with different Ga loadings after 1 h on stream. Pure flame-made TiO_2 showed about the same ethane conversion (24%) as observed with the empty reactor tube (23%), indicating that TiO_2 was virtually inactive after 1 h on stream. Ethane and CO_2 conversions as well as ethene yield showed a maximum at a gallium loading of ca. 10 wt %. The maximum ethene yield was 22%, corresponding to 57% ethane conversion at 38% selectivity to ethene. The only significant byproduct detected in addition to coke formation was methane (only traces of C_3 were observed), similar to the observation of Nakagawa et al.[8] The increase in ethane conversion with increasing Ga loading indicates that Ga_2O_3 is crucial for catalytic activity. However, the undesired formation of methane and carbon deposits also indicates its potential role in alkane cracking. Carbon deposition on the catalyst surface increased with increasing Ga loading, as indicated by the thermoanalytical results shown in Figure 7b. At high Ga loading the catalyst surface was fully covered by carbon deposits and the catalyst activity and selectivity became similar to those of pure TiO_2.

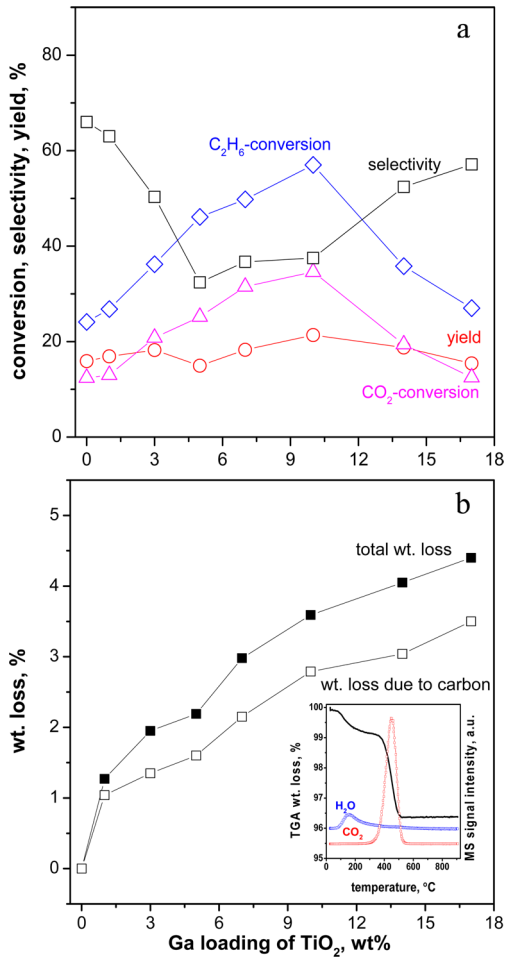

Figure 7. (a) Effect of Ga loadings on the oxidative dehydrogenation of ethane. Conditions: total gas flow, 15 mL/min; CO_2/C_2H_6 ratio, 2.5; space velocity, 6000 L/((kg of cat.) h); temperature, 700 °C. (b) TGA analysis of mass loss due to water desorption and burning of carbon deposit of spent Ga-loaded TiO_2 catalysts as a function of Ga loading. Inset: mass loss and MS signal of 10% Ga/TiO_2.

Carbon dioxide conversion showed a behavior similar to that of ethane conversion when the Ga loading was increased. This indicates active participation of CO_2 during the reaction partially by removal of deposited carbon from the catalyst surface via reverse Boudouard reaction.[14] However, at higher Ga loadings (>10 wt %), the rate of carbon deposition apparently surpasses its removal by oxidation with CO_2, leading to rapid and complete coverage and thus blocking of the active surface sites. These changes in CO_2 conversion also lead to variation in the amount of CO in each experiment. A strong decrease in ethane conversion from 57% to 24% was observed in the absence of CO_2, which means when CO_2 was replaced by He in the reactor feed over the 10% Ga/TiO_2 catalysts, indicating the beneficial role of CO_2 in this reaction system.

Figure 7b shows how carbon deposition increased with the Ga loading. Interestingly, the catalyst with optimal Ga loading (10 wt % Ga/TiO_2) showed a rate of deactivation lower than that observed by Nakagawa et al.,[9] maintaining 22% ethene yield in comparison to 18% after 1 h time on stream. Nakagawa et al.[8] showed that an increase in surface area of Ga_2O_3 increases the ethene yield. Therefore, the observed high initial catalytic activity can be assigned to the high initial surface area of the flame-made catalysts (~120 m^2/g) and enhanced sintering resistance in the presence of Ga.

However, Ga_2O_3 seems to be very active for ethane ODH as well as ethene cracking. Figure 8 shows the interdependence of selectivity and conversion with progressive time on stream. After 20 min of reaction, almost all Ga/TiO_2 catalysts showed similar conversion (83%) and selectivity (10%) values. However, conversion decreased due to active site blocking by coke with a concomitant increase in selectivity. These curves corroborate that the 10% Ga/TiO_2 showed the best performance among the tested catalysts.

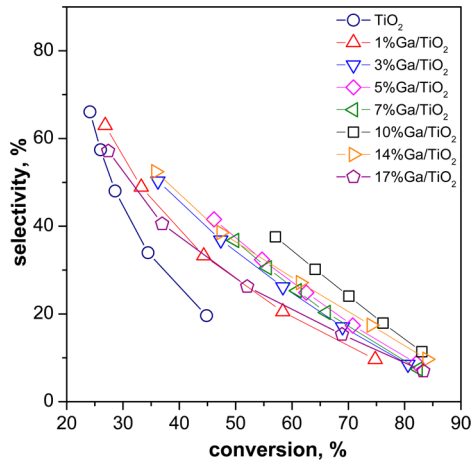

Figure 8. Selectivity vs conversion of various Ga-loaded TiO_2 catalysts with progressing reaction time. Conditions: total gas flow, 15 mL/min; CO_2/C_2H_6 ratio, 2.5; space velocity, 6000 L/((kg of cat.) h); temperature, 700 °C; data taken, 20–60 min of the reaction, first point after 20 min of reaction and the rest after 10 min from high to low conversion.

In Scheme 1, both observed (solid lines) and expected (broken lines) reaction pathways during ODHE are depicted. Reaction with only ethane mixed with helium showed formation of ethene, CH_4, and coke, indicating the existence

DOI: 10.1021/cs500685d
ACS Catal. 2015, 5, 690–702

Scheme 1. Observed (Solid Lines) and Expected (Broken Lines) Reaction Pathways during ODHE: (a) Dehydrogenation of Ethane; (b–d) Coking Reactions; (e) Reverse Boudouard Reaction; (f) Reverse Water-Gas Shift Reaction; (g) Steam Reforming of Ethane[a]

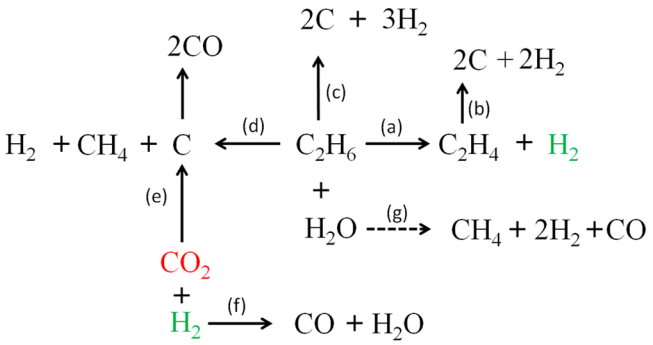

[a]CO_2 (red) is expected to consume H_2 (green) from ethane dehydrogenation.

of pathways a, c, and d. The weight loss obtained from TGA of the spent catalysts in the absence of CO_2 was found to be higher (3.3%) than that in its presence (2.8%). This indicates that more coke was formed in the absence of CO_2, proving that CO_2 mitigates coke deposition and likely oxidizes the deposited coke during the ODHE reaction (pathway e). TGA measurement showed that oxidation of coke by CO_2 (total weight loss about 2.7%) was efficient in the temperature window of 800–1000 °C, similar to the behavior reported by Nakagawa et al.[9] The weight loss due to coke removal up to 700 °C was only 0.24%, while the rest (2.46%) was only removed at higher temperatures. A large amount of carbon deposits (O_2/Ar oxidation of coke) was also obtained from reaction with a mixture of ethene and CO_2 (3.6%), corroborating the existence of pathway b. To confirm the significance of the reverse water-gas shift (RWGS) reaction, ethane was replaced by H_2, keeping other reaction conditions similar. Under these conditions CO_2 conversion was about 14% with CO as a major detectable product (pathway f) and the presence of traces of CH_4 indicated the significance of methanation. H_2O produced from the RWGS reaction is also expected to follow steam reforming of ethane (pathway g). The significance of these reactions probably strongly depends on catalyst composition and reaction conditions. Reactions b–d especially seem to be enhanced at higher Ga loadings (>10 wt %), leading to enhanced catalyst deactivation.

3.3. Influence of Reaction Conditions on Performance of Optimal Catalyst. Figure 9 shows the effect of reaction temperature on the behavior of the best-performing 10% Ga/TiO_2 catalyst. Conversion increased almost linearly with increasing reaction temperature, similar to the findings of Nakagawa et al.,[8] while CO_2 conversion showed a maximum around 700 °C. Ethene selectivity was higher at lower reaction temperature (600 °C), reaching a flat minimum between 650 and 700 °C and then increasing to 68% at 800 °C. The increase in ethane conversion with increasing temperature can be attributed to gradual evolution of thermal dehydrogenation of ethane,[48] potentially enhanced by CO_2.[49] The lowering of CO_2 conversion at higher reaction temperatures (>700 °C) could be attributed to the rapid deactivation of the catalyst due to the inability of CO_2 to oxidize and gasify the deposited carbon at a sufficient rate. High temperature accelerates the formation and

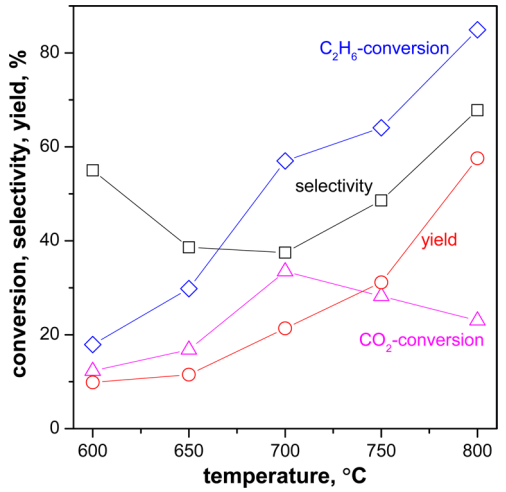

Figure 9. Influence of temperature on the catalytic performance of 10% Ga/TiO_2. Conditions: total gas flow, 15 mL/min; CO_2/C_2H_6 ratio, 2.5; space velocity, 6000 L/((kg of cat.) h).

deposition of carbon on the catalyst surface.[11] The high ethane conversion at high temperatures (>700 °C) is mainly attributed to thermal dehydrogenation.

High selectivity at high temperatures (800 °C) arises from the unavailability of active surface sites for further oxidation of ethene due to enhanced coking. Though a high reaction temperature seems favorable due to high ethane conversion and ethene selectivity, it causes massive carbon deposition on the catalyst surface and also on the reactor wall, requiring extensive cleaning, which is expected to increase costs of production.[4]

Figure 10 shows the effect of the molar ratio of carbon dioxide to ethane in the feed on the catalytic performance of

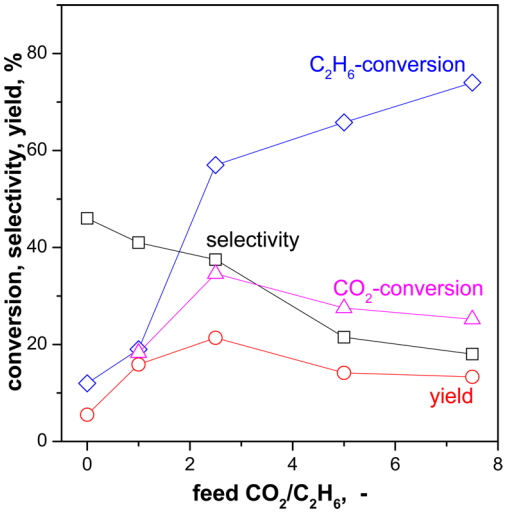

Figure 10. Influence of CO_2/C_2H_6 feed ratio on the catalytic performance of 10% Ga/TiO_2. Conditions: total gas flow, 15 mL/min; CO_2/C_2H_6 ratio, 2.5; space velocity, 6000 L/((kg of cat.) h); temperature, 700 °C.

the 10% Ga/TiO_2 catalyst. The measurements were carried out wih the space velocity kept constant (6000 L/((kg of cat.) h)) at 700 °C. In the absence of CO_2, both the yield and conversion were 12% and 5.5%, respectively, proving the active participation of CO_2 in the reaction. The conversion increased with increasing CO_2/C_2H_6 ratio, whereas the ethene selectivity

DOI: 10.1021/cs500685d
ACS Catal. 2015, 5, 690–702

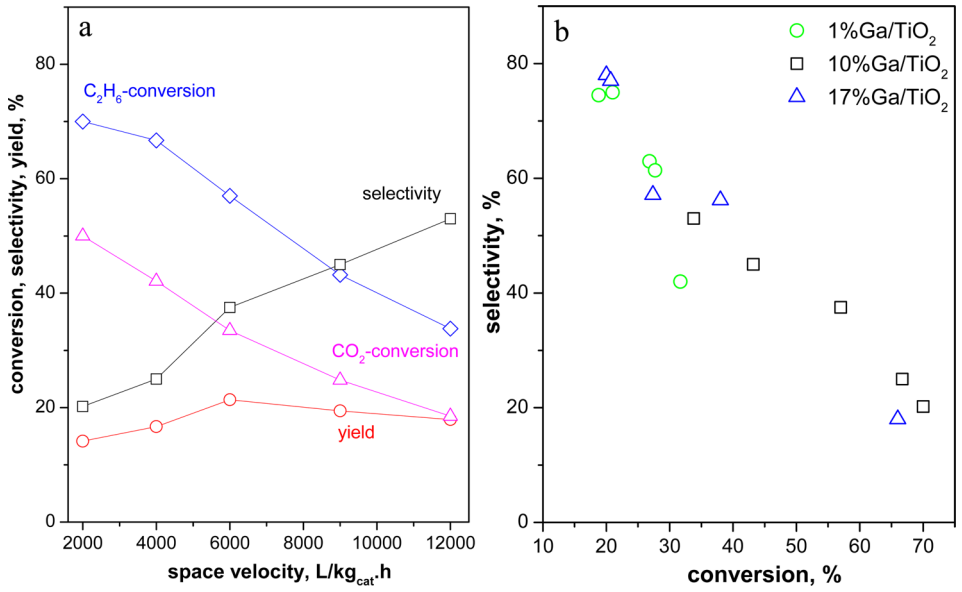

Figure 11. (a) Influence of space velocity on the catalytic performance of 10% Ga/TiO_2 and (b) selectivity versus conversion of fresh Ga/TiO_2 catalysts containing 1, 10, and 17% of Ga (space velocity 2000−12000 L/((kg of cat.) h)), both at 700 °C with a CO_2/C_2H_6 ratio of 2.5.

decreased strongly. This reduction in ethene selectivity is attributed to deep oxidation of ethene and/or cracking.[50] Under the conditions given, a molar CO_2/C_2H_6 ratio of 2.5 seemed to be optimal, resulting in a maximum ethene yield of 22%.

Figure 11 shows the influence of the space velocity on the performance of the 10% Ga loaded TiO_2 catalyst. Ethane and CO_2 conversions showed a similar dependence on the space velocity. The ethene yield slightly decreased with higher space velocity as a result of the counteracting effects of decreasing ethane and CO_2 conversion and increasing ethene selectivity. Increasing the space velocity resulted in higher ethene selectivity, reaching 53% at a space velocity of 12000 L/((kg of cat.) h). The selectivity increase at higher space velocity is ascribed to lower hydrocracking and deep oxidation of ethene. High CO_2 conversion at lower space velocities indicates an enhanced removal of coke, consequently exposing the active sites of the catalyst responsible for high C_2H_6 conversions. This role of CO_2 as an oxidant in the removal of coke as CO has been well documented.[9,51] Figure 11b shows decreasing selectivity with increasing conversion, indicating the existence of consecutive reactions of the desired product (ethene). The catalytic performance of these samples seemed to be similar, indicating that differences in selectivity might be only due to changes in conversion, due to coke deposition.

In addition to the study of the influence of the reaction conditions, we also investigated the effect of thermal pretreatment of the optimal 10% Ga/TiO_2 catalyst on its performance. For this purpose as-prepared catalysts were calcined at different temperatures (700, 800, and 900 °C) with a ramp rate of 10 °C/min and held at the target temperature for 1 h. The intensity of the main rutile reflection (2θ = 27°) increased with increasing calcination temperature, while that of anatase (2θ = 25°) gradually disappeared (Figure 12a). This indicates that Ga could not suppress rutile formation at higher calcination temperatures (700−900 °C), in contrast to the observation of Depero et al.[24] and Benjaram et al.[31] with catalysts prepared by laser-induced pyrolysis and wet chemistry, respectively, where >90% anatase was present up to a calcination temperature of 800 °C. Moreover, defects in the crystal structure of TiO_2 during flame synthesis (Figure 1a), which were absent in powders made by laser-induced pyrolysis and wet chemistry, might have favored the anatase to rutile transformation at lower temperatures. New reflections corresponding to Ga_2O_3 were observed at 2θ = 30, 32, 33, and 35° only after calcining the powder at 900 °C, implying that high temperatures are required to transform amorphous Ga_2O_3 to a crystalline phase. Similar observation was reported by Depero et al.,[24] where crystalline Ga_2O_3 was discernible only after calcining Ga-loaded TiO_2 at 1000 °C.

Catalytic results indicated a gradual reduction in ethene yield with increasing calcination temperature until 800 °C (not shown). However, the sample calcined at 900 °C afforded an ethene yield (20%) similar to that of the as-prepared 10% Ga/TiO_2 (22%) at a space velocity of 6000 L/((kg of cat.) h). However, the ethane conversion decreased from 57 to 38%. The selectivity versus conversion plot (Figure 12b) shows that at isoconversion there is no significant difference in the performance of these catalysts. Therefore, the differences in selectivity may be only due to different conversions. However, at the same space velocity (e.g., 6000 L/((kg of cat.) h)), the low ethane conversion of the calcined samples can be attributed to this thermal pretreatment, which induced changes in the physicochemical properties of the catalyst as its surface area decreased from 120 to 24 m^2/g and crystalline Ga_2O_3 was formed (Figure 12a) after calcination at 900 °C. These results indicate that high dispersion of Ga_2O_3 is essential for achieving optimal catalyst activity. Such dispersion is facilitated during the co-synthesis of Ga/Ti oxides by flame aerosol technology.[16,44]

3.4. Carbon Deposition and Catalyst Regeneration. Severe coking on the catalyst surface is the major reason for its deactivation, requiring further investigation. Raman spectroscopy (Figure 6b) and thermal analyses (Figure 7b) were applied to identify and quantify the deposited carbon on spent catalysts. Additionally, insight on the time dependent carbon deposition was also gained. The intensity of the D band of carbon deposits on pure TiO_2 (not shown) was smaller in comparison to that of the G band; however, with higher Ga

DOI: 10.1021/cs500685d
ACS Catal. 2015, 5, 690−702

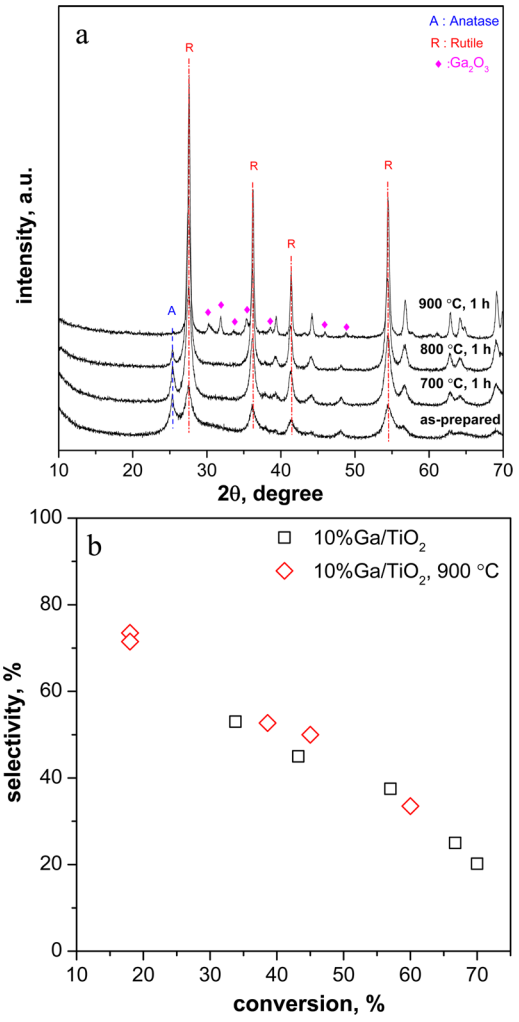

Figure 12. (a) XRD patterns of 10% Ga/TiO_2 calcined at various temperatures. (b) Selectivity versus conversion of fresh (black squares) and calcined (red diamonds) (900 °C for 1 h) 10% Ga/TiO_2 catalysts. Conditions: total gas flow, 15 mL/min; CO_2/C_2H_6 ratio, 2.5; space velocity, 2000−12000 L/((kg of cat.) h); temperature, 700 °C.

loading the intensities of both bands became similar (Figure 6b). The D bands were broader than the G bands in all spent catalysts, and no major effect of Ga content on the type of deposited carbon was observed. The amount of carbon belonging to D and G bands was estimated from the ratio of the areas under the 1356 and 1605 cm^{-1} peaks, respectively. The fraction of D-type carbon was always higher on Ga-loaded catalysts and showed a D/G ratio of ∼1.66 that remained nearly constant up to 10 wt % Ga and slightly decreased upon further Ga addition. An estimation of the particle size of the deposited carbon using the intensities of D and G bands[47,52] indicated particles in the range of 4.5−5.4 nm.

Figure 7b shows the amount of deposited carbon as a function of gallium content of the Ga-loaded TiO_2 derived from TGA analysis. Mass spectroscopy (MS) was used to analyze the gaseous species evolving during the thermal analysis. The MS signal along with mass loss as a function of temperature was plotted to identify the species responsible for the mass change (inset, Figure 7b). All spent Ga-containing catalysts showed a two-step mass loss (H_2O loss between 80 and 200 °C and carbon loss between 300 and 520 °C). No noticeable weight loss was observed with spent TiO_2, indicating no significant amount of carbon (Figure 7b) on its surface.

Carbon deposited primarily on the Ga_2O_3 surface or at the Ga_2O_3−TiO_2 interface, as increasing weight loss was observed with increasing Ga content. The mass loss due to carbon increased from 1.04 to 3.5% in spent catalysts containing 1 and 17 wt % of gallium, respectively. A nearly linear relationship between deposited carbon and nominal gallium content was observed (Figure 7b). Moreover, a small upshift in carbon oxidation temperature (∼50 °C) with increasing Ga loading was observed. The upshift of the onset of the oxidation could be attributed to the higher carbon amount on the catalyst surface.[53] This increasing amount of carbon on the catalyst surface with increasing Ga loading is responsible for the observed stronger loss of activity of higher Ga-loaded catalysts.

Figure 13a shows the amount of carbon deposition and ethane conversion as a function of time on stream for the 10% Ga/TiO_2. Carbon deposition on the catalyst increased almost linearly, reaching a saturation level after 60 min on stream, while ethane conversion decreased steadily until 120 min on stream. Note that the ethane conversion of 25% after 120 min is similar to that obtained if the reaction is performed in the empty reactor tube (23.1%), suggesting that the catalyst was virtually inactive after this time. Raman spectra of the catalysts

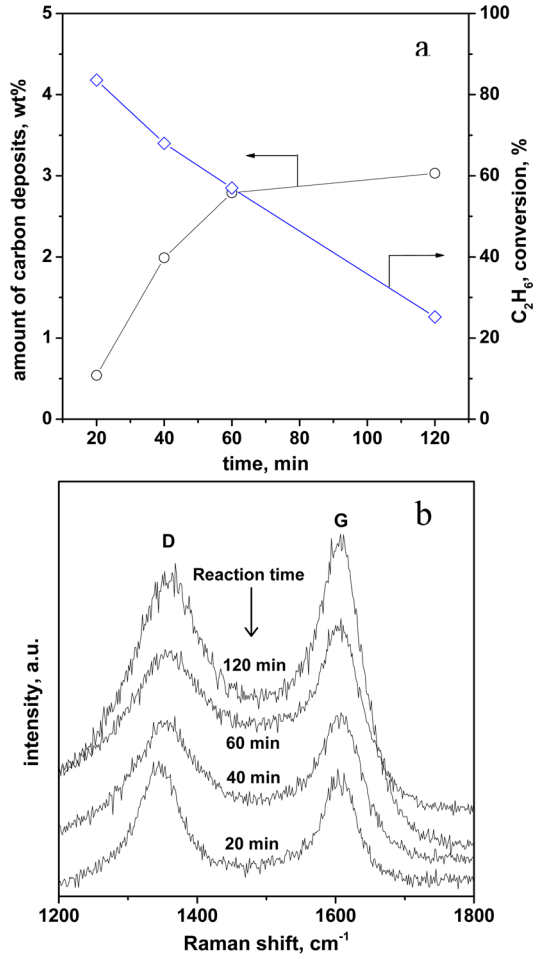

Figure 13. (a) Influence of reaction time (time on stream) on the amount of carbon deposition on 10% Ga/TiO_2. (b) Corresponding Raman spectra. Conditions: total gas flow, 15 mL/min; CO_2/C_2H_6 ratio, 2.5; space velocity, 6000 L/((kg of cat.) h); temperature, 700 °C.

DOI: 10.1021/cs500685d
ACS Catal. 2015, 5, 690−702

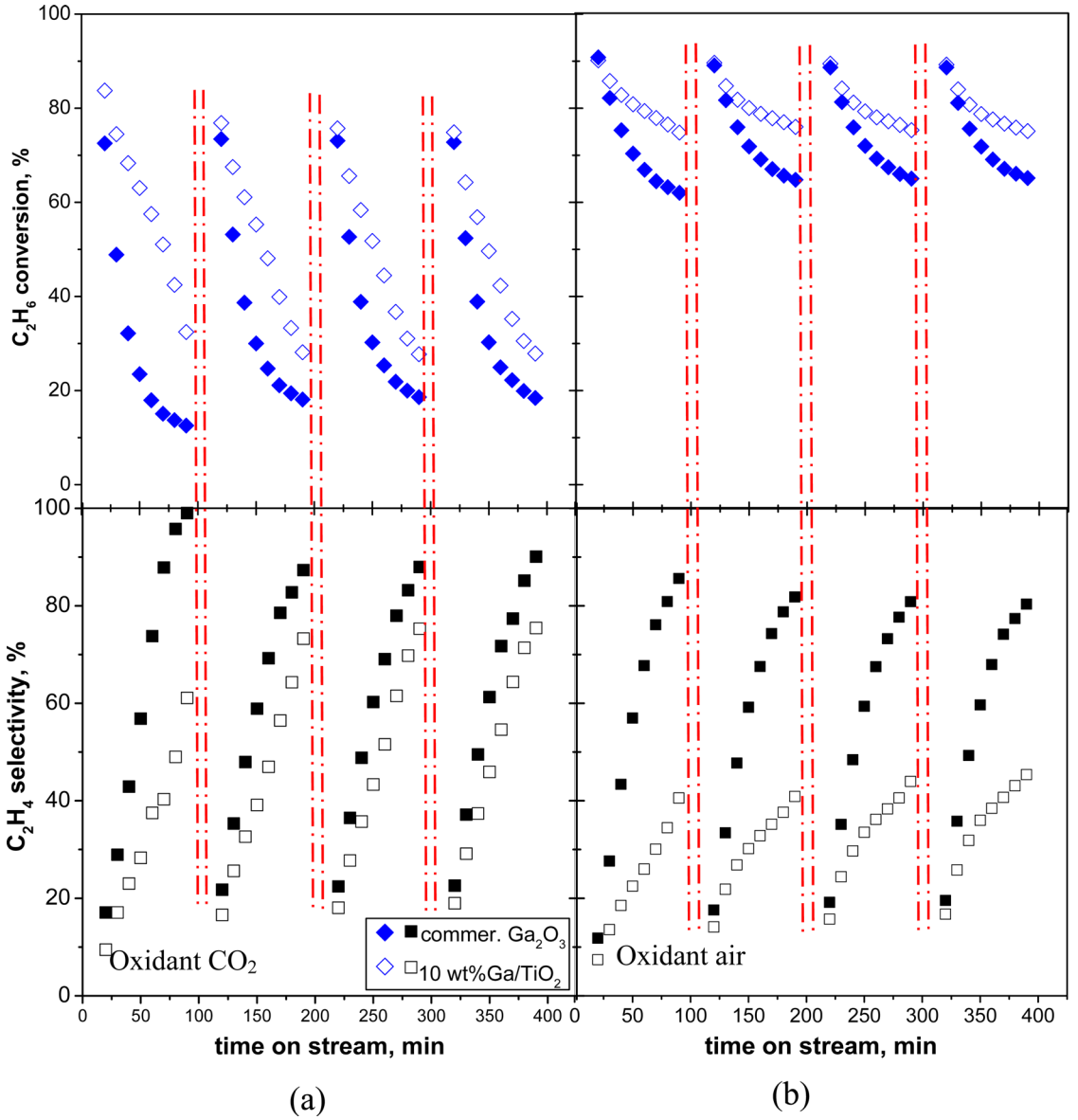

Figure 14. Catalyst regeneration tests of 10% Ga/TiO_2 and commercial Ga_2O_3 with air for 10 min after 90 min reaction with different oxidants in the feed: (a) CO_2/C_2H_6; (b) air/C_2H_6. Conditions: total gas flow, 15 mL/min; (CO_2 or air)/C_2H_6 ratio, 2.5; space velocity, 6000 L/((kg of cat.) h); temperature, 700 °C. The period between the red dotted lines represents regeneration in air.

after different times on stream (Figure 13b) showed that at all times both types of carbon, D and G, are present on the catalyst. The size of carbon particles ranged from 4.2 to 5.1 nm, on the basis of calculations utilizing the intensities of the specific D and G bands.[47,52] However, as mentioned before, it appears that the change in catalyst activity was dependent on the amount of deposited carbon rather than on its particle size. Overall, it is deduced that carbon deposition is the major cause for the loss in catalyst performance.

The regeneration of the flame-made 10% Ga/TiO_2 catalyst was accomplished by oxidizing (gasifying) the carbon deposits using synthetic air after each cycle (90 min time on stream). The 10% Ga/TiO_2 catalyst exhibited good regenerability, as it nearly regained its initial conversion (83.7%) even at such a short regeneration time (10 min) (Figure 14a). The small loss in activity after the first regeneration might be due to some early loss in surface area or loss of some temporary active sites.[14] Gradual reduction in ethane conversion with time on stream is associated with continuing deposition and accumulation of carbon on the active sites of the catalyst. This increase in coking results from the insufficient ability of CO_2 to remove coke from the catalyst surface.[14] Similar behavior was observed with the commercial Ga_2O_3; however, the deactivation rate was much faster, exhibiting lower ethane conversion compared to10% Ga/TiO_2. Commercial Ga_2O_3 showed an ethene selectivity >90%, whereas >60% selectivity was achieved with 10% Ga/TiO_2 at the end of the first cycle. After regeneration, the selectivity of the Ga_2O_3 decreased (87%), whereas that of 10% Ga/TiO_2 increased to 70%, which remained almost constant even after the third regeneration. The high activity of 10% Ga/TiO_2 is attributed to the high dispersion of Ga on the TiO_2. The increase in selectivity with time indicates that the density of active sites decreases due to coke deposition, thereby slowing down the desired and particularly the undesired reactions. For both catalysts the major cause for the continuous

DOI: 10.1021/cs500685d
ACS Catal. 2015, 5, 690−702

reduction in ethane conversion with time is coke deposition on the catalyst surface.

Further investigations on the regenerability of the catalysts were performed by replacing the oxidant CO_2 in the feed with air, keeping the other aforementioned reaction parameters constant. A high rate of decoking is expected due to the use of air, resulting in high activity. Both commercial Ga_2O_3 and the 10% Ga/TiO_2 catalysts showed very high initial conversion (around 90%); however, the activity also declined with time on stream (Figure 14b), but less rapidly. Upon regeneration, both catalysts almost regained their initial conversion values. Though both of them showed higher activity with air as oxidant, the selectivity to ethene was much lower (~40%), even after 90 min time on stream in comparison to that of the reaction performed using CO_2 as oxidant (around 80%). In addition to ethene, methane, CO_2, and CO were also detected in the product stream. The high ethane conversion with low ethene selectivity can be attributed to their total oxidation by air. Similar to the previous regenerability test with CO_2, the gradual decline in catalyst activity is attributed to coking. In both cases, ethene selectivity improved with time on stream (increasing coking), indicating a decrease of active sites responsible for both the desired and undesired reactions. The Raman spectra of these spent catalysts were comparable to those recorded for experiments with CO_2 as oxidant, showing a similar ratio of D and G bands. Overall, though coking reduced the performance of both the Ga_2O_3 and 10% Ga/TiO_2, the use of the latter as a catalyst seems beneficial due to its higher performance even with a relatively low loading of gallium.

4. CONCLUSION

Flame synthesis of Ga-loaded (0−17 wt %) TiO_2 results in spherical, virtually nonporous particles of about 10 nm diameter in which the Ga constituent is well dispersed. Ga loadings up to about 8 wt % lead to a strong decrease of the population of acidic sites, while a further increase of the Ga content has little effect on the acidic site population but alters the distribution of their strength. The strongest acidic sites are most prominent on the highly Ga loaded catalysts. The population of basic sites changes relatively little with Ga loading. These materials show remarkable catalytic activity in the oxidative dehydrogenation of ethane (OHDE) with CO_2 as oxidant. While flame-made pure titania is nearly inactive, the catalytic performance of Ga-loaded TiO_2 increases strongly with increasing Ga content up to about 10 wt %, affording an ethene yield of 22%. Higher Ga loading proved to be unfavorable, due to enhanced cracking and carbon deposition. In addition to Ga loading, the feed ratio CO_2/C_2H_6, temperature, and space velocity in the tubular fixed-bed microreactor were found to be crucial for achieving optimal ethene yield. Ethane conversion and ethene selectivity showed a clear interdependence, higher ethane conversion resulting in lower ethene selectivity. Raman spectra revealed the presence of both D- and G-type carbon in all of the spent catalysts. This carbon deposition leads to enhanced ethene selectivity due to decreased ethane conversion. The deactivated catalysts could be easily regenerated by air in a short time (10 min) at a reaction temperature of 700 °C. If air was used instead of CO_2 as oxidant in the reaction, carbon deposition was lower, resulting in less prominent catalyst deactivation. However, with air as oxidant, the selectivity to ethene was much lower due to enhanced further oxidation of ethene, affording significantly lower ethene yield in comparison to the reaction with CO_2. The ease and efficiency of the catalyst regeneration may provide a base for developing a dynamic process consisting of alternative reaction/regeneration cycles.

AUTHOR INFORMATION

Corresponding Author

*A.B.: e-mail, baiker@chem.ethz.ch; tel, +41 44 632 31 53; fax, +41 44 632 11 63.

Notes

The authors declare no competing financial interest.

ACKNOWLEDGMENTS

This work was financially supported by ETH Research Grant ETH-39-12-2, and the European Research Council under the European Union's Seventh Framework Program (FP7/2007-2013, ERC grant agreement no. 247283) is kindly acknowledged.

REFERENCES

(1) Cavani, F.; Trifirò, F. *Catal. Today* **1995**, *24*, 307−313.
(2) Gärtner, C. A.; van Veen, A. C.; Lercher, J. A. *ChemCatChem* **2013**, *5*, 3196−3217.
(3) Zimmermann, H.; Walzl, R. *Ullmann's Encyclopedia of Industrial Chemistry*; Wiley-VCH: Weinheim, Germany, 2000.
(4) Ren, T.; Patel, M.; Blok, K. *Energy* **2006**, *31*, 425−451.
(5) Kung, H. H. *Advances in Catalysis*; Elsevier: Amsterdam, 1994; Vol. *40*, pp 1−38.
(6) Ansari, M. B.; Park, S.-E. *Energy Environ. Sci.* **2012**, *5*, 9419−9437.
(7) Nakagawa, K.; Okamura, M.; Ikenaga, N.; Suzuki, T.; Kobayashi, T. *Chem. Commun.* **1998**, 1025−1026.
(8) Nakagawa, K.; Kajita, C.; Ide, Y.; Okamura, M.; Kato, S.; Kasuya, H.; Ikenaga, N.; Kobayashi, T.; Suzuki, T. *Catal. Lett.* **2000**, *64*, 215−221.
(9) Nakagawa, K.; Kajita, C.; Okumura, K.; Ikenaga, N.; Nishitani-Gamo, M.; Ando, T.; Kobayashi, T.; Suzuki, T. *J. Catal.* **2001**, *203*, 87−93.
(10) Petre, A. L.; Auroux, A.; Gélin, P.; Caldararu, M.; Ionescu, N. I. *Thermochim. Acta* **2001**, *379*, 177−185.
(11) Michorczyk, P.; Ogonowski, J. *Appl. Catal. A: Gen.* **2003**, *251*, 425−433.
(12) Shen, Z.; Liu, J.; Xu, H.; Yue, Y.; Hua, W.; Shen, W. *Appl. Catal. A: Gen.* **2009**, *356*, 148−153.
(13) Xu, B.; Zheng, B.; Hua, W.; Yue, Y.; Gao, Z. *J. Catal.* **2006**, *239*, 470−477.
(14) Zheng, B.; Hua, W.; Yue, Y.; Gao, Z. *J. Catal.* **2005**, *232*, 143−151.
(15) Mädler, L.; Kammler, H. K.; Mueller, R.; Pratsinis, S. E. *J. Aerosol Sci.* **2002**, *33*, 369−389.
(16) Strobel, R.; Pratsinis, S. E. *J. Mater. Chem.* **2007**, *17*, 4743−4756.
(17) Strobel, R.; Baiker, A.; Pratsinis, S. E. *Adv. Powder Technol.* **2006**, *17*, 457−480.
(18) Rudin, T.; Pratsinis, S. E. *Ind. Eng. Chem. Res.* **2012**, *51*, 7891−7900.
(19) Ernst, F. O.; Kammler, H. K.; Roessler, A.; Pratsinis, S. E.; Stark, W. J.; Ufheil, J.; Novák, P. *Mater. Chem. Phys.* **2007**, *101*, 372−378.
(20) van Vegten, N.; Baidya, T.; Krumeich, F.; Kleist, W.; Baiker, A. *Appl. Catal. B: Environ.* **2010**, *97*, 398−406.
(21) Schimmoeller, B.; Pratsinis, S. E.; Baiker, A. *ChemCatChem.* **2011**, *3*, 1234−1256.
(22) Strobel, R.; Stark, W. J.; Mädler, L.; Pratsinis, S. E.; Baiker, A. *J. Catal.* **2003**, *213*, 296−304.
(23) Spurr, R. A.; Myers, H. *Anal. Chem.* **1957**, *29*, 760−762.
(24) Depero, L. E.; Marino, A.; Allieri, B.; Bontempi, E.; Sangaletti, L.; Casale, C.; Notaro, M. *J. Mater. Res.* **2000**, *15*, 2080−2086.
(25) Shannon, R. *Acta Crystallogr., Sect. A* **1976**, *32*, 751−767.
(26) Akhtar, K. M.; Pratsinis, S. E.; Mastrangelo, S. V. R. *J. Mater. Res.* **1994**, *9*, 1241−1249.

DOI: 10.1021/cs500685d
ACS Catal. 2015, 5, 690−702

(27) Vemury, S.; Pratsinis, S. E. *J. Am. Ceram. Soc.* **1995**, *78*, 2984−2992.
(28) Teoh, W. Y.; Amal, R.; Mädler, L.; Pratsinis, S. E. *Catal. Today* **2007**, *120*, 203−213.
(29) Wegner, K.; Pratsinis, S. E. *AlChE J.* **2003**, *49*, 1667−1675.
(30) Mohammadi, M. R.; Fray, D. J. *Acta Mater.* **2007**, *55*, 4455−4466.
(31) Reddy, B. M.; Ganesh, I.; Reddy, E. P.; Fernández, A.; Smirniotis, P. G. *J. Phys. Chem. B* **2001**, *105*, 6227−6235.
(32) Auroux, A.; Gervasini, A. *J. Phys. Chem.* **1990**, *94*, 6371−6379.
(33) Bartholomew, C. H. *Appl. Catal. A: Gen.* **2001**, *212*, 17−60.
(34) Campelo, J. M.; Lafont, F.; Marinas, J. M.; Ojeda, M. *Appl. Catal. A: Gen.* **2000**, *192*, 85−96.
(35) Liu, Z. F.; Tabora, J.; Davis, R. J. *J. Catal.* **1994**, *149*, 117−126.
(36) Shibata, K.; Kiyoura, T.; Kitagawa, J.; Sumiyoshi, T.; Tanabe, K. *Bull. Chem. Soc. Jpn.* **1973**, *46*, 2985−2988.
(37) Gervasini, A.; Auroux, A. *J. Therm. Anal.* **1991**, *37*, 1737−1744.
(38) Tsyganenko, A. A.; Pozdnyakov, D. V.; Filimonov, V. N. *J. Mol. Struct.* **1975**, *29*, 299−318.
(39) Primet, M.; Pichat, P.; Mathieu, M. V. *J. Phys. Chem.* **1971**, *75*, 1216−1220.
(40) Ristić, M.; Popović, S.; Musić, S. *Mater. Lett.* **2005**, *59*, 1227−1233.
(41) Yamazoe, S.; Okumura, T.; Hitomi, Y.; Shishido, T.; Tanaka, T. *J. Phys. Chem. C* **2007**, *111*, 11077−11085.
(42) Busca, G. *Phys. Chem. Chem. Phys.* **1999**, *1*, 723−736.
(43) Chen, M.; Xu, J.; Su, F. Z.; Liu, Y. M.; Cao, Y.; He, H. Y.; Fan, K. N. *J. Catal.* **2008**, *256*, 293−300.
(44) Pushkar, Y. N.; Sinitsky, A.; Parenago, O. O.; Kharlanov, A. N.; Lunina, E. V. *Appl. Surf. Sci.* **2000**, *167*, 69−78.
(45) Mädler, L.; Stark, W. J.; Pratsinis, S. E. *J. Mater. Res.* **2002**, *17*, 1356−1362.
(46) Porto, S. P. S.; Fleury, P. A.; Damen, T. C. *Phys. Rev.* **1967**, *154*, 522−526.
(47) Knight, D. S.; White, W. B. *J. Mater. Res.* **1989**, *4*, 385−393.
(48) Burch, R.; Crabb, E. M. *Appl. Catal. A: Gen.* **1993**, *97*, 49−65.
(49) Choudhary, V. R.; Mondal, K. C.; Mulla, S. A. R. *J. Chem. Sci.* **2006**, *118*, 261−267.
(50) Baidya, T.; Vegten, N.; Baiker, A. *Top. Catal.* **2011**, *54*, 881−887.
(51) Krylov, O. V.; Mamedov, A. K.; Mirzabekova, S. R. *Ind. Eng. Chem. Res.* **1995**, *34*, 474−482.
(52) Jawhari, T.; Roid, A.; Casado, J. *Carbon* **1995**, *33*, 1561−1565.
(53) Monti, D. A. M.; Baiker, A. *J. Catal.* **1983**, *83*, 323−335.

DOI: 10.1021/cs500685d
ACS Catal. 2015, 5, 690−702